This article has been accepted for inclusion in a future issue of this journal. Content is final as presented, with the exception of pagination.

Practical Finite-Time Observer-Based Adaptive Backstepping Super-Twisting Sliding Mode Control for Deep-Sea Hydraulic Manipulator

Gang Chen, *Member, IEEE*, Wei Wu, *Student Member, IEEE*, Chenguang Yang, *Fellow, IEEE*, Huosheng Hu, *Life Senior Member, IEEE*, Jingjing Zhang, Jianwei Shi, Chuanyu Wu, and Yu Ma

***Abstract*—Parameter uncertainties and unknown disturbances always exist in the trajectory tracking control of a deep-sea hydraulic manipulators (DHMs), significantly reducing tracking accuracy. To address these issues, a practical finite-time observer-based adaptive backstepping super-twisting sliding mode control method (PFTO-ABSTC) is proposed for precise DHM tracking control. First, a projection-type adaptive law is constructed to handle the parameter uncertainties. In addition, Levant's Differentiator is employed to obtain velocity of the DHM and construct the adaptive law regression vector, minimizing system noise from differentiation and filtering operations. Second, a practical finite-time observer (PFTO) strategy is proposed to estimates lump disturbances and compensates them in the controller, avoiding high-gain phenomenon of the controller effectively. Then, the PFTO-ABSTC controller is proposed by integrating the backstepping technique, which chattering-free property can be achieved. In addition, the uncertainties and disturbances of the DHM dynamics are well addressed in the closed-loop system, and asymptotic tracking performance can be guaranteed by Lyapunov theory. Finally, comparative experimental results validate the effectiveness of the proposed control strategy. Experimental results show that the proposed method can achieve smaller control errors and better control performance than the ESO-ABSTC, ABSTC, and PID control methods, and the maximum control errors are improved by at least 41.30%, 50.76%, and 66.67%, respectively.**

***Index Terms*—Backstepping technique, deep-sea hydraulic manipulator (DHM), finite-time observer, nonlinear systems, sliding mode control.**

Received 27 August 2024; revised 4 December 2024; accepted 22 January 2025. This work was supported in part by the National Natural Science Foundation of China under Grant 52275037, Grant 51875528, and Grant 41506116, in part by Zhejiang Provincial Natural Science Foundation of China under Grant LR24E050002, in part by the Key Research and Development Project of Zhejiang Province under Grant 2023C03015 and Grant 2024C01257, in part by the Emergency Management Research and Development Project of Zhejiang Province under Grant 2024YJ026, in part by the Key Research and Development Project of Ningxia Hui Autonomous Region under Grant 2023BDE03002, and in part by the Fundamental Research Funds of Zhejiang Sci-Tech University under Grant 24242088-Y. *(Corresponding authors: Gang Chen; Chenguang Yang.)*

Gang Chen is with the School of Mechanical Engineering, Zhejiang Sci-Tech University, Hangzhou 310018, China, also with Donghai Laboratory, Zhoushan 316021, China, and also with Zhejiang Marine Intelligent Ship Institute, Hangzhou 310015, China (e-mail: gchen@zstu.edu.cn).

Wei Wu is with the School of Mechanical Engineering, Zhejiang Sci-Tech University, Hangzhou 310018, China (e-mail: 202220501051@mails.zstu.edu.cn).

Chenguang Yang is with the Department of Computer Science, University of Liverpool, L69 3BX Liverpool, U.K. (e-mail: cyang@ieee.org).

Huosheng Hu is with the School of Computer Science and Electronic Engineering, University of Essex, CO4 3SQ Colchester, U.K. (e-mail: hhu@essex.ac.uk).

Jingjing Zhang and Jianwei Shi are with Zhejiang CathayBot Technology Company Ltd., Jinhua 321035, China (e-mail: jack.zhang@cathaybot.com; jianwei.shi@cathaybot.com).

Chuanyu Wu is with Zhejiang Ocean University, Zhoushan 316022, China, and also with the School of Mechanical Engineering, Zhejiang Sci-Tech University, Hangzhou 310018, China (e-mail: cywu@zstu.edu.cn).

Yu Ma is with the Department of Electrical and Electronic Engineering, Ningxia University, Yinchuan 750021, China (e-mail: may@nxu.edu.cn).

Digital Object Identifier 10.1109/TIE.2025.3541284

I. Introduction

DEEP-SEA hydraulic manipulators have gained considerable attention in recent decades because of their numerous advantages, including high power-to-density ratio, rapid response characteristics, and significant loading capacity [1], [2]. These manipulators are commonly used as actuators on various types of deep-sea submersibles to carry out heavy-load operational tasks. Therefore, achieving precise control of DHM is crucial in specific scenarios such as deep-sea exploration, cable laying, and subsea rescue operations. However, conventional PID control methods face significant challenges in achieving motion control of DHM in the presence of uncertain model parameters, as there are high levels of nonlinearity [3], strong coupling [4], [5], and time-varying parameters [6] inherent in hydraulic systems. These factors include variations in the oil temperature affecting the effective bulk modulus of the hydraulic fluid and changes in transmission efficiency due to wear in mechanical transmission structures, among other factors. Furthermore, the precise motion control for DHM is further complicated by the presence of multiple sources of unknown disturbances [7].

With the rapid development of the modern control theory, nonlinear control methods have emerged as a focal point of

This article has been accepted for inclusion in a future issue of this journal. Content is final as presented, with the exception of pagination.

research. Various nonlinear control methods, such as adaptive control (AC) [8], [9], adaptive robust control (ARC) [10], [11], sliding mode control (SMC) [12], [13], and neural network control (NNC) [14], [15], have been proposed to address the high-precision control challenges of complex electromechanical systems. In particular, adaptive control methods, which leverages the effectiveness of adaptive principles in addressing time-varying system parameter, have been developed to achieve precise control of electrohydraulic servo systems [16]. Moreover, discontinuous mapping adaptive control methods were proposed in [17] and validated through experiments on hydraulic actuators. However, DHM inevitably encounter unknown disturbances from both the internal and external environment in practical applications, making it difficult to predict disturbance bounds and posing a greater challenge for controller design. Although adaptive control methods typically rely on sufficiently large controller gains to mitigate the negative effects of system disturbances [5], [17], this approach can lead to undesirable dynamic and steady-state performance of the system.

Thus, to minimize the adverse effects of disturbances, an effective approach is to estimate the unknown lump disturbances and incorporate disturbance compensation in the controller design process. This method has the potential to enhance robustness and tracking performance without the need for excessively large controller gains. In [18], an extended state observer-based composite state controller was proposed to limit performance degradation of the system in the presence of external disturbances. Another study [19] proposed an active disturbance rejection control method to achieve precise motion control of continuous wave pulse generators in the presence of multiple disturbances. However, these studies rely only on proportional terms as feedback signals for the controller, which indicates the need for improvement in disturbance rejection performance and pose challenges in applying it to DHM facing multiple disturbances. Given the advantages of SMC, such as strong robustness, fast convergence, and ease of implementation, the combination of observer with SMC has gained significant research attention in the control of electrohydraulic servo systems. In [20], Zhang et al. designed a global integral SMC to increase the trajectory tracking accuracy of electrohydraulic servo systems by integrating a global integral sliding mode surface design with an improved extended state observer (ESO). Won et al. proposed a high-gain observer-based integral SMC strategy to achieve position tracking control of electrohydraulic servo systems, reducing the control gain of the controller and effectively suppressing system chattering phenomena [21].

Although the integration of ESO can mitigate the chattering phenomena commonly associated with traditional SMC, the presence of discontinuous terms still leads to residual chattering in the system. To increase the disturbance estimation capacity and further eliminate chattering phenomena in SMC, a novel approach that combines the super-twisting SMC method with ESO has been proposed [12]. Ding et al. proposed a synthesized super-twisting SMC method based on disturbance estimation to enhance the control performance and disturbance rejection capability of permanent magnet synchronous motors [22]. Another study [23] proposed a super-twisting SMC method combined with disturbance compensation to achieve precise trajectory tracking control of electrohydraulic servo systems by estimating system disturbances via a state observer and compensating for them in the controller. Although traditional ESO-based methods have achieved certain control effects, their estimated errors exhibit only asymptotic convergence characteristics, which inevitably lead to lower estimation speed and accuracy. Additionally, if model uncertainties become the major influencing factor of system disturbances, observers designed on the basis of nominal system models may suffer from severe performance degradation, thus affecting the overall control performance of the controller. Therefore, it is crucial to design an effective control strategy that can achieve precise motion control of DHM under the influence of unknown disturbances and model parameters uncertainties, which is an important issue that requires further investigation.

Inspired by the aforementioned problems, this article proposes a practical finite-time observer-based adaptive backstepping super-twisting sliding mode control (PFTO-ABSTC) method to further address the precise trajectory tracking control of DHM with parameter uncertainties and unknown external disturbances. The contributions of this article can be summarized as follows:

1) Unlike the ESO in [12], [23], the PFTO strategy is proposed to estimate and compensate the lumped disturbances, which can be guaranteed the practical finite-time convergence of the estimated error.

2) A PFTO-ABSTC controller is developed for the DHMs, which can be achieved chattering-free property. The parameter uncertainties and disturbances of the DHM dynamics are well addressed in the controller, which enhances the disturbance rejection ability.

3) The asymptotic tracking performance of the controller can be guaranteed in theory. The experimental validation was conducted, which demonstrate the excellent performance of the proposed control strategy.

The remainder of this article is organized as follows. Section II establishes the dynamic model of the DHM. Section III designs the PFTO-ABSTC controller and provides a stability proof for the system. The experimental results and analysis are presented in Section IV. Finally, conclusions are drawn in Section V.

II. Dynamics Modeling and Probelms Formation

A. Dynamics of the Manipulator

Considering an n-DOF DHM in Fig. 1(a), the dynamics of the manipulator are considered as follows:

$$M(q)\ddot{q} + C(q,\dot{q})\dot{q} + H(\dot{q})\dot{q} + G(q) = \tau + D \tag{1}$$

where q, $\dot{q}$ and $\ddot{q}$ represent the position, velocity, and acceleration of the joint angle of the manipulator, respectively. $M \in R^{n\times n}$, $C \in R^{n\times n}$, and $G \in R^{n\times 1}$ represents the symmetric positive definite inertia matrix, coriolis and centrifugal force matrix, and gravity matrix of the manipulator, respectively. $H \in R^{n\times n}$ represents the hydrodynamics, including viscous drag and added mass effects [1]. τ represents the torque vector

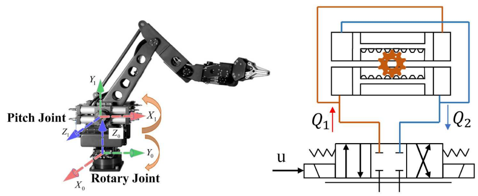

(a) (b)

Fig. 1. Architecture of the deep-sea hydraulic manipulator system. (a) Deep-sea Hydraulic Manipulator. (b) Hydraulic Actuator.

of the manipulator; D represents unmodeled disturbances such as friction force and interference during the movement of the manipulator.

Remark 1: Due to the constraints in manufacturing costs and internal installation space, DHMs typically has only position sensors and pressure sensors. The Levant's differentiator (LD), which have the simple and noise amplification free structure [24], thus it is chosen for obtain the velocity signal of the system. Its specific structure is as follows:

$$\begin{aligned} \dot{m}_0 &= v \\ v &= -\ell_1 |m_0 - q|^{1/2} sign(m_0 - q) + m_1 \\ \dot{m}_1 &= -\ell_2 sign(m_1 - v) \end{aligned} \tag{2}$$

where q is the input signal of the LD, that is, the position signal of the manipulator; m_0 and m_1 are the status signal; ℓ_1 and ℓ_2 are the designed parameters; v is the output signal, that is, the velocity signal obtained by the LD.

Lemma 1 [25]: Assuming that the input signal of the LD satisfies $|m_0 - q| \le \varepsilon_1$ and the appropriate ℓ_1 and ℓ_2 are selected, then in finite time t_{TD}, the LD will satisfy:

$$|m_0 - q| \le \varsigma_1 \varepsilon_1 = \xi_1, |v - \dot{q}| \le \varsigma_2 \varepsilon_1^{1/2} = \xi_2 \tag{3}$$

where $\varsigma_1, \varsigma_2 > 0$ and which are constants that depend on the design parameters of the LD.

B. Dynamics of the Hydraulic System

As shown in Fig. 1(b), the joint of the manipulator studied in this article realizes the rotation motion of the joint by controlling the servo valve. Define $y = \text{diag}[y_1, y_2, \ldots, y_n]$ represents the move distance of the hydraulic cylinder at different joints. Assuming that there is no internal leakage in the whole hydraulic system, the dynamic equation of the hydraulic system can be modeled as follows:

$$\begin{aligned} \frac{V_{01} + Ay}{\beta_e} \dot{P}_1 &= -A \frac{\partial y}{\partial q} \dot{q} + Q_1 \\ \frac{V_{02} - Ay}{\beta_e} \dot{P}_2 &= A \frac{\partial y}{\partial q} \dot{q} - Q_2 \end{aligned} \tag{4}$$

where V_{01}, V_{02} represents the initial volume of the oil inlet chamber and the oil return chamber of the hydraulic cylinder, respectively; βe represents the effective bulk modulus of hydraulic oil; $P_1 = [P_{11}, P_{12}, \ldots, P_{1n}]^T$, $P_2 = [P_{21}, P_{22}, \ldots, P_{1n}]^T$ represent the pressure of the oil cylinder inlet chamber and return chamber, respectively; $\dot{P}_1$, $\dot{P}_2$ represents the pressure change rates of the P_1 and P_2, respectively; $A = \text{diag}[A_1, A_2, \ldots, A_n]$ represents the effective stamping area of the oil inlet chamber and the oil return chamber of cylinder; $(\partial y / \partial q)$ represents the complete differential matrix between cylinder movement and joint angle can be written as

$$\frac{\partial y}{\partial q} = \begin{bmatrix} \frac{\partial y_1}{\partial q_1} & \cdots & \frac{\partial y_1}{\partial q_n} \\ \cdots & \cdots & \cdots \\ \frac{\partial y_n}{\partial q_1} & \cdots & \frac{\partial y_n}{\partial q_n} \end{bmatrix} \tag{5}$$

and Q_1, Q_2 represents the fluid flow rates of the oil inlet chamber and the oil return chamber of the hydraulic cylinder, the relationship between it and the servo valve input signal can be established as follows:

$$\begin{aligned} Q_1 &= k_q g_1(P_1, u) u \\ Q_2 &= k_q g_2(P_2, u) u \end{aligned} \tag{6}$$

where k_q represents the proportional coefficient between the input signal of the servo valve and the flow rate. The relationship $g_1(P_1, u), g_2(P_2, u)$ between the control signal and the flow rate can be established as follows:

$$\begin{aligned} g_1(P_1, u) &= n(u)\sqrt{P_s - P_1} + n(-u)\sqrt{P_1 - P_r} \\ g_2(P_2, u) &= n(u)\sqrt{P_2 - P_r} + n(-u)\sqrt{P_s - P_2} \end{aligned} \tag{7}$$

where P_s and P_r represents the oil supply pressure and return pressure of the hydraulic system, respectively. The function $n(\Xi)$ in (7) is defined as follows:

$$n(\Xi) = \begin{cases} 1, if\ \Xi \ge 0 \\ 0, if\ \Xi < 0 \end{cases} \tag{8}$$

Through the above process, the torque τ of the manipulator can be written as

$$\tau = \frac{\partial y}{\partial q}(AP_1 - AP_2). \tag{9}$$

C. State Space Model

According to the above dynamic modeling process, the control goal of this article is to make each joint of the manipulator track the desired trajectory $x_d = q_d = [q_{d1}, q_{d2}, \ldots, q_{dn}]^T$ as accurately as possible by designing a controller. Define the state vector $x = [x_1^T, x_2^T, x_3^T]^T = \left[q^T, \dot{q}^T, (AP_1 - AP_2)^T\right]^T$. According to (1), (2), (4), and (9), the state space model of DHM dynamics can be established as follows:

$$\begin{aligned} \dot{x}_1 &= x_2 \\ \dot{x}_2 &= -\phi_1 x_2 + \theta_1 \phi_2 x_3 - \phi_3 + f_1 \\ \dot{x}_3 &= -\theta_2 \phi_4 x_2 + \theta_3 \phi_5 u + f_2 \end{aligned} \tag{10}$$

where $\phi_1 = M(q)^{-1}(C(q, v) + H(v))$, $\phi_2 = M^{-1}$, $\phi_3 = M^{-1} G(q)$, $\phi_4 = [(1/V_{01} + Ay) + (1/V_{02} - Ay)]$, $\phi_5 = [(g_1(P_1, u)/V_{01} + Ay) + (g_2(P_2, u)/V_{02} - Ay)]$, $\theta_1 = (\partial y / \partial q)$, $\theta_2 = A(\partial y / \partial q)\beta e$, $\theta_3 = \beta e k_q$, $f_1 = M^{-1}[D - C(q, (\dot{q} - v))\dot{q} - H(\dot{q} - v)\dot{q}] + \Pi_1$ and $f_2 = \Pi_2$, which Π_i represents disturbances during modeling process.

Assumption 1: The uncertain disturbances f_1 and f_2 are both bounded and their change rates are bounded.

Assumption 2 [7]: The parametric uncertainties is bounded by the known range, i.e., $\theta \in \Omega_\theta = \{\theta : \theta_{\min} \le \theta \le \theta_{\max}\}$.

This article has been accepted for inclusion in a future issue of this journal. Content is final as presented, with the exception of pagination.

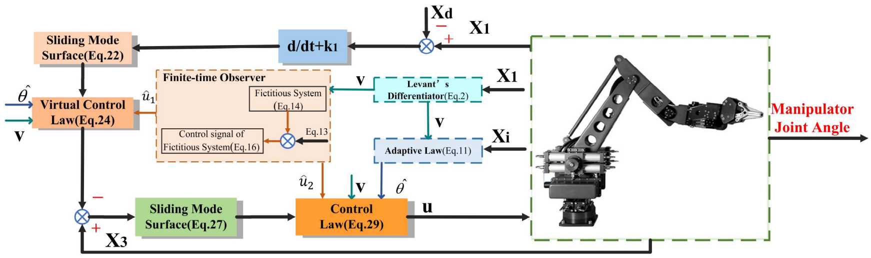

Fig. 2. Block diagram of the PFTO-ABSTC.

III. PFTO-ABSTC Controller Design

In this section, an PFTO-ABSTC controller is established for precise motion control of DHM, including three main components: projection-type adaptive law, PFTO and controller design. The overall structural diagram is shown in Fig. 2.

A. Projection-Type Adaptive Law

Define $\hat{\bullet}$ as the estimated value of $\bullet$ and define estimate error $\tilde{\bullet} = \bullet - \hat{\bullet}$. Define $\Theta = [\theta_1, \theta_2, \theta_3]^T$, and a projection-type adaptive law is designed as follows [26], [27]:

$$\dot{\hat{\Theta}} = \Pr oj_{\hat{\Theta}}(\Gamma N) \tag{11}$$

where $\Gamma = \mathrm{diag}\{\Gamma_1, \Gamma_2, \Gamma_3\}$ represents the positive definite adaptive gain matrix; $N \in R^3$ is the adaptive vector, which will be designed in the following chapters. The projection mapping is defined as follows:

$$\Pr oj_{\hat{\Theta}}(\bullet) = \begin{cases} 0, & \hat{\theta} = \theta_{\max} \quad and \quad \bullet > 0 \\ 0, & \hat{\theta} = \theta_{\min} \quad and \quad \bullet < 0 \\ \bullet, & otherwise \end{cases}. \tag{12}$$

B. Practical Finite-Time Observer

In this part, PFTO strategy is constructed to estimate lumped disturbances and achieves practical finite-time stability. To maintain generality, the state space model of system (10) is reconstructed and can be express as

$$\dot{x}_{i+1} = \chi_i(x, \phi) + \Theta\varphi_i + f_i \tag{13}$$

where φ_i represents the polynomial matrix of known form, χ_i represents the known formal equation and f_i represents the disturbance, $i = 1, 2$. To estimate the disturbance f_i, a fictitious system is constructed according to (13) as follows:

$$\dot{\hat{x}}_{i+1} = \chi_i(x, \phi) + \hat{\Theta}\varphi_i + \hat{u}_i \tag{14}$$

where $\hat{x}_{i+1}$ represent the state of the fictitious system, $\hat{u}_i$ represents the input signal of the fictitious system. According to (13) and (14), the following expression for the estimated error can be obtained as follows:

$$\dot{\tilde{x}}_{i+1} = \tilde{\Theta}\varphi_i + f_i - \hat{u}_i. \tag{15}$$

Thus, if $\left\|\dot{\tilde{x}}_{i+1}\right\| = 0$ and $\left\|\tilde{x}_{i+1}\right\| = 0$ is satisfied, we can consider that the control signal $\hat{u}_i$ of the fictitious system is the disturbance value of the practical system, that is, $\left\|\tilde{\Theta}\varphi_i + f_i - \hat{u}_i\right\| = 0$. Therefore, the process of constructing the estimation strategy is transformed into the control signal $\hat{u}_i$ of the fictitious system in the subsequent part. Thus, the control signal $\hat{u}_i$ of the fictitious system is designed as follows:

$$\begin{cases} \hat{u}_i = \hat{\eta}_i + k_{f1}\tilde{x}_{i+1} + k_{f2}|\tilde{x}_{i+1}|^{(r-1)/r} sign(\tilde{x}_{i+1}) \\ \dot{\hat{\eta}}_i = \omega_1\tilde{x}_{i+1} - \omega_2\hat{\eta}_i \end{cases} \tag{16}$$

where k_{f1}, k_{f2}, ω_1 and ω_2 both are positive definite diagonal matrices; r is the positive constant which satisfied $r > 2$; η_i is the adaptive term. In addition, define $\tilde{\eta}_i = \eta_i - \hat{\eta}_i = \tilde{\Theta}\varphi_i + f_i - \hat{\eta}_i$. According to (16), the rate of change of the estimated error is expressed as follows:

$$\dot{\tilde{\eta}}_i = \frac{d}{dt}(\tilde{\Theta}\varphi_i + f_i) - \dot{\hat{\eta}}_i = \dot{\eta}_i - \omega_1\tilde{x}_{i+1} + \omega_2\eta_i - \omega_2\tilde{\eta}_i. \tag{17}$$

Lemma 2 [28]: For any $\wp_1 > 0$, $0 < \iota < 1$ and $0 < \wp_2 < \infty$, an extended Lyapunov condition with practical finite-time stability can be given as $\dot{V}(x) + \wp_1 V^{\iota}(x) \le \wp_2$, where the settling time can be estimated by $T_r \le t_0 + (1/\wp_1\wp_3(1-\iota))\left[V^{1-\iota}(x(0)) - ((\wp_2/\wp_1(1-\iota)))^{(1-\iota)/\iota}\right]$ and $0 < \wp_3 < 1$.

Lemma 3 [29]: For any variables ℓ_1 and ℓ_2, $|\ell_1|^{\lambda_1}|\ell_2|^{\lambda_2} \le \lambda_1\lambda_3|\ell_1|^{\lambda_1+\lambda_2}\Big/(\lambda_1+\lambda_2)+\lambda_2\lambda_3^{-\lambda_1/\lambda_2}|\ell_2|^{\lambda_1+\lambda_2}\Big/(\lambda_1+\lambda_2)$ can obtained, which λ_1, λ_2 and λ_3 are all positive constants.

Theorem 1: According to assumptions 1 and 2, if the lumped disturbance $\tilde{\Theta}\varphi_i + f_i$ of the system satisfies $|\eta_i| \le D_1$ and $(d/dt)\,|\dot{\eta}_i| \le D_2$, then the state estimated error $\tilde{x}_{i+1}$ and the disturbance estimated error $\tilde{\eta}_i$ of the observer is practical finite-time stable.

Proof: See Appendix A.

Remark 2: Since the DHM always lacks velocity feedback signal, the input signal of the PFTO is v when the unmatched disturbance f_1 is estimated, and it is not difficult to conclude that the convergence time of estimating the unmatched disturbance f_1 through the above PFTO is $\max\{t_{LD}, t_{PFTO}\}$. Therefore, by combining LD, the convergence time of the PFTO strategy proposed in this part is further written as $T_s = \max\{t_{LD}, t_{PFTO}\}$.

C. Controller Design

Define trajectory tracking errors $z_1 = x_1 - x_{1d}$ and $\alpha_1 = \dot{x}_{1d} - k_1 z_1$, where x_{1d} is the expected tracking signal of the manipulator joint; k_1 is a positive definite diagonal matrix; α_1 is a virtual control law about x_1. Define filter error z_2 to facilitate subsequent analysis and calculation as follows:

$$z_2 = \dot{z}_1 + k_1 z_1 = x_2 - \alpha_1 \tag{18}$$

This article has been accepted for inclusion in a future issue of this journal. Content is final as presented, with the exception of pagination.

*Step*1: Position Tracking. Taking the derivative of z_2 in (18) yields the following:

$$\begin{aligned}\dot{z}_2 &= \dot{x}_2 - \dot{\alpha}_1\\ &= -\phi_1 x_2 + \theta_1\phi_2 x_3 - \phi_3 + f_1 - \dot{\alpha}_1\end{aligned} \tag{19}$$

and integral-type sliding mode manifold is defined as follows:

$$s_1 = z_2 + \int_0^t a_1 z_2 d\tau \tag{20}$$

where a_1 is a positive definite diagonal matrix. Combined with (19), the derivation of the sliding mode manifold (20) can be obtained as follows:

$$\begin{aligned}\dot{s}_1 &= \dot{z}_2 + a_1 z_2\\ &= -\phi_1 x_2 + \theta_1\phi_2 x_3 - \phi_3 + f_1 - \dot{\alpha}_1 + a_1 z_2.\end{aligned} \tag{21}$$

According to (21), the virtual control law α_2 is designed as follows:

$$\begin{aligned}\alpha_2 &= \frac{1}{\hat{\theta}_1\phi_2}(\alpha_{2a} + \alpha_{2s} + \alpha_{2aux})\\ \alpha_{2a} &= \phi_1 v + \phi_3 - \hat{u}_1 + \dot{\alpha}_1 - a_1 z_2\\ \alpha_{2s} &= -k_{11}s_1 - k_{12}|s_1|^{1/2}sign(s_1)\\ \dot{\alpha}_{aux} + \Im_1\alpha_{aux} &= -k_{13}sign(s_1)\end{aligned} \tag{22}$$

and k_{11}, k_{12}, k_{13}, and $\Im_1$ both are positive definite diagonal matrix.

*Step*2: Pressure Tracking. Define $z_3 = x_3 - \alpha_2$ and taking the derivative of z_3 can yield the following:

$$\dot{z}_3 = \dot{x}_3 - \dot{\alpha}_2 = -\theta_2\phi_4 x_2 + \theta_3\phi_2 u + f_2 - \dot{\alpha}_2. \tag{23}$$

Due to the unmeasurable velocity signal x_2 was existed in the α_2, thus it cannot be directly calculated and brought into the controller design process. In order to solve this practical problem, the derivative of the virtual control law α_2 consists of the following two parts [5]:

$$\begin{aligned}\dot{\alpha}_2 &= \dot{\alpha}_{2c} + \dot{\alpha}_{2u}\\ \dot{\alpha}_{2c} &= \frac{\partial\alpha_2}{\partial t} + \frac{\partial\alpha_2}{\partial x_1}x_{2d} + \frac{\partial\alpha_2}{\partial x_2}\dot{x}_{2d}\\ \dot{\alpha}_{2u} &= \frac{\partial\alpha_2}{\partial x_2}[-\phi_1(x_2 - v) + \theta_1\phi_2 z_3 - a_1 z_2\\ &\quad + \alpha_{2s} + \alpha_{2aux} + \tilde{\theta}_1\phi_2 x_3 + f_1 - \hat{u}_1] + \frac{\partial\alpha_2}{\partial\hat{\theta}}\dot{\hat{\theta}}\end{aligned} \tag{24}$$

where $\dot{\alpha}_{2c}$ represents the computable part of the $\dot{\alpha}_2$, and $\dot{\alpha}_{2u}$ represents the undifferentiable part caused by disturbance, unmeasurable state and other factors, which will be processed by the sliding mode controller.

The integral-type sliding mode manifold is defined as follows:

$$s_2 = z_3 + \int_0^t a_2 z_3 d\tau \tag{25}$$

where a_2 is the positive definite diagonal matrix. The derivation of the sliding mode manifold (25) can be obtained:

$$\dot{s}_2 = -\theta_2\phi_4 x_2 + \theta_3\phi_5 u + f_2 - \dot{\alpha}_2 + a_2 z_3. \tag{26}$$

According to (26), the the control law u can be obtained as follows:

$$\begin{aligned}u &= \frac{1}{\hat{\theta}_3\phi_5}(u_a + u_s + u_{aux})\\ u_a &= \hat{\theta}_2\phi_4 v - \hat{u}_2 + \dot{\alpha}_{2c} - a_2 z_3\\ u_s &= -k_{21}s_2 - k_{22}|s_2|^{1/2}sign(s_2)\\ \dot{u}_{aux} + \Im_2 u_{aux} &= -k_{23}sign(s_2)\end{aligned} \tag{27}$$

and k_{21}, k_{22}, k_{23}, $\Im_2$ both are positive definite diagonal matrix.

Theorem 2: Assuming that $\left|d(\phi_1\xi_1 + \tilde{f}_1 + \hat{\theta}_2 z_3)/dt\right| \le D_3$ and $\left|d(\hat{\theta}_2\phi_4\xi_1 + \tilde{f}_2)/dt\right| \le D_4$ are satisfied, according to the design of the virtual control law α_2 and the control law u, choosing large enough gain of the controller to make the following matrix Υ_{1i} and matrix Υ_{2i} ((29), shown at the bottom of the page) are positive definite:

$$\Upsilon_{1i} = \begin{bmatrix}\varpi_{1i}k_{i1} & 0 & 0\\ 0 & 2\varpi_{2i}k_{i1}+k_{i1}^3 & -\left(\varpi_{2i}+k_{i1}^2+\frac{k_{i1}\Im_i}{2}\right)\\ 0 & -\left(\varpi_{2i}+k_{i1}^2+\frac{k_{i1}\Im_i}{2}\right) & 2\varpi_{3i}\Im_i+k_{i1}+\Im_i\end{bmatrix} \tag{28}$$

where $D \in \max\{D_3, D_4\}$. Then, the system converges to the sliding mode manifold in finite time.

Proof: See Appendix B.

Theorem 3: The gain and parameters are controlled by appropriate adjustments to make the following matrix

$$\Lambda = \begin{bmatrix}\Lambda_1 & 0 & \Lambda_2 & \Lambda_3 & 0\\ 0 & \mathrm{diag}[k_{f1}\omega_1, \omega_2]I_4 & 0 & 0 & 0\\ \Lambda_2 & 0 & \frac{\lambda_{\min}(\Upsilon_{11})}{\lambda_{\max}(\Phi_1)}I_4 & 0 & 0\\ \Lambda_3 & 0 & 0 & \frac{\lambda_{\min}(\Upsilon_{12})}{\lambda_{\max}(\Phi_2)}I_4 & 0\\ 0 & 0 & 0 & 0 & \lambda_{\min}(\psi)\end{bmatrix} \tag{30}$$

is the positive definite matrix, where $\Lambda_1 = \begin{bmatrix}k_1 & -(1/2) & 0\\ -(1/2) & a_1 & 0\\ 0 & 0 & a_2\end{bmatrix}$, $\Lambda_2 = \begin{bmatrix}0 & 0 & 0\\ -(k_{12}/2) & -k_{11} & (1/2)\\ 0 & 0 & 0\end{bmatrix}$, $\Lambda_3 = \begin{bmatrix}0 & 0 & 0\\ 0 & 0 & 0\\ -(k_{22}/2) & -(k_{21}/2) & -(1/2)\end{bmatrix}$, I_4 represents a positive definite matrix of dimension 4. In addition, the adaptive law in (11) is obtained by using the following adaptive equation:

$$N = \begin{bmatrix}\phi_1 x_3 z_2 & -\phi_4\nu z_3 & \phi_5 u z_3\end{bmatrix}^T - \psi\hat{\Theta} \tag{31}$$

$$\Upsilon_{2i} = \begin{bmatrix}\varpi_{1i}k_{i2} + k_{i2}^3 + k_{i2}k_{i3} - k_{i2}D & -\frac{k_{i1}k_{i2}^2+k_{i1}k_{i3}+k_{i1}D}{2} & \frac{2\varpi_{3i}k_{i3}-\varpi_{1i}+k_{i3}-2\varpi_{3i}D-D}{2}\\ -\frac{k_{i1}k_{i2}^2+k_{i1}k_{i3}+k_{i1}D}{2} & 2\varpi_{2i}k_{i2} - k_{i1}^2k_{i2} & k_{i1}k_{i2} + \frac{k_{i2}\Im_i}{2}\\ \frac{2\varpi_{3i}k_{i3}-\varpi_{1i}+k_{i3}-2\varpi_{3i}D-D}{2} & k_{i1}k_{i2} + \frac{k_{i2}\Im_i}{2} & -k_{i2}\end{bmatrix} \tag{29}$$

This article has been accepted for inclusion in a future issue of this journal. Content is final as presented, with the exception of pagination.

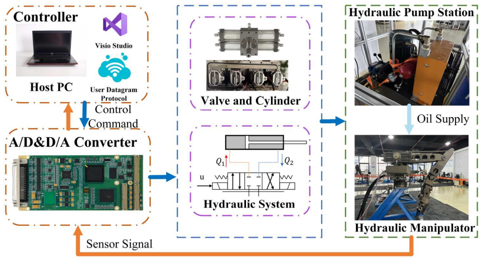

Fig. 3. Experimental platform.

where $\psi = \mathrm{diag}[\psi_1, \psi_2, \psi_3]$ is a positive definite matrix. Thus, the PFTO-ABSTC controller can ensure that all signals of the closed-loop system are bounded and that the tracking error can asymptotically converge, that is, $t \to \infty, z_1 \to 0$.

Proof: See Appendix C.

IV. Experimental Verify

A. Experimental Steup

The experimental setup, as shown in Fig. 3, primarily consists of a 2-degree-of-freedom (2-DOF) DHM platform, a control system, and a signal conversion system. The experiments were conducted at the rotary joint and pitch joint, as depicted in Fig. 1. The manipulator joints provide position and pressure feedback to the PC host. The PC host uses the controller proposed in this article to compute the control signals. These digital signals are then converted into analog signals for the servo valve through the signal conversion system. By controlling the servo valve's opening, the manipulator joints are driven. The entire experimental platform operates with a sampling period of 5 ms, and the hydraulic system is supplied with a pressure of 13 Mpa.

The effectiveness of the proposed method is verified by comparing the four controllers in three sets of experiments:

$C1$: PFTO-ABSTC proposed in this article. The controller parameters are tuned as: $k_1 = \mathrm{diag}[50, 45]$, $k_{11} = \mathrm{diag}[500, 300]$, $k_{12} = \mathrm{diag}[200, 170]$, k_{13}=diag$[100, 100]$, $\Im_1 = \mathrm{diag}[30, 20]$, $k_{21} = \mathrm{diag}[2000, 1500]$, $k_{22} = \mathrm{diag}[770, 650]$, $k_{23} = \mathrm{diag}[500, 400]$, $\Im_2 = \mathrm{diag}[50, 45]$, $\Gamma = \mathrm{diag}[5.0 \times 10^{-4}, 4.2 \times 10^{-4}, 0.08, 0, 05, 20, 35]$; k_{f1}=diag$[100, 80, 50, 55]$, k_{f2}= diag$[50, 60, 35, 35]$, $r = \mathrm{diag}[3, 2, 2, 4]$, $\omega_1 = \mathrm{diag}[110, 100, 65, 70]$, and $\omega_2 = \mathrm{diag}[225, 210, 175, 190]$. Parameter adjustment guidelines can be seen in [12].

$C2$: ESO-ABSTC, which is integrated the ABSTC control method with ESOs proposed in [18], [26]. The controller values were set the same as those of C1, and the ESOs parameters are set as: $\omega_{e1} = \mathrm{diag}[100, 150]$, $\omega_{e2} = \mathrm{diag}[120, 115]$.

$C3$: ABSTC without any disturbance compensation. The controller gains were set as: $k_1 = \mathrm{diag}[50, 45]$, $k_{11} = \mathrm{diag}[1500, 2000]$, $k_{12} = \mathrm{diag}[500, 430]$, $k_{13} = \mathrm{diag}[100, 100]$, $\Im_1 = \mathrm{diag}[30, 20]$, $k_{21} = \mathrm{diag}[11000, 9800]$, $k_{22} = \mathrm{diag}[1000, 1120]$, $k_{23} = \mathrm{diag}[1000, 600]$, $\Im_2 = \mathrm{diag}[50, 45]$.

$C4$: PID: proportional-integral-derivative controller with $k_p = \mathrm{diag}[75, 225]$, $k_I = \mathrm{diag}[25, 10]$, and $k_D = \mathrm{diag}[0, 0]$.

Furthermore, the following three performance evaluation metrics are introduced: 1) Absolute maximum error (AME): $AME = \max\{|z_1(i)|\}$; 2) Mean squared error (MSE): $MSE = (1/n)\sum_{i=1}^{n}(z_1(i) - \bar{z}_1(i))^2$; 3) Standard Deviation: (SD): $SD = \sqrt{\sum_{i=1}^{n}(z_1(i) - \bar{z}_1)^2/n}$, where i is the sampling point, z_1 is the trajectory tracking error, and $\bar{z}_1$ is the mean trajectory error.

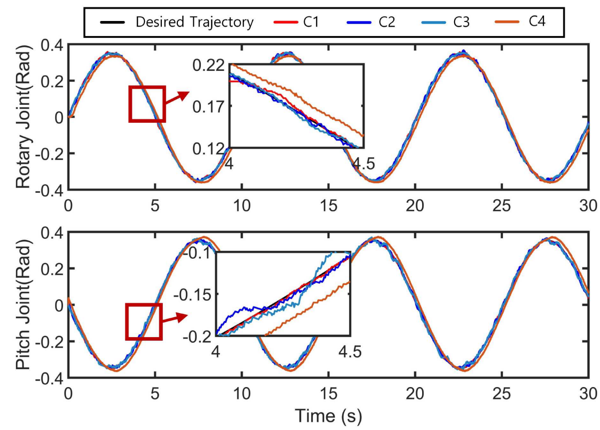

Fig. 4. Trajectory tracking results of the four controllers in Case 1.

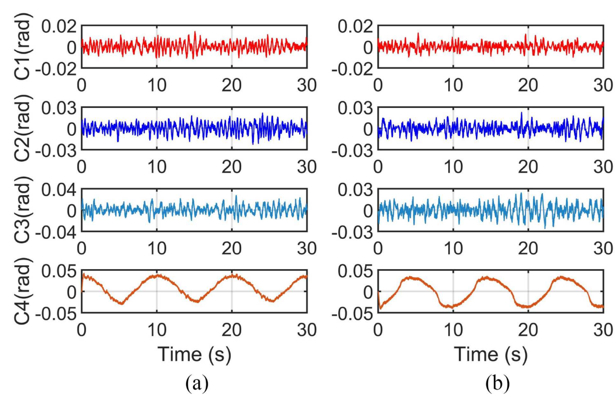

Fig. 5. Trajectory tracking errors of the four controllers in Case 1. (a) Rotary Joint. (b) Pitch Joint.

B. Experimental Result

*Case*1: Low-speed sine trajectory $x_{11d} = 0.35\sin(0.6t)rad$ and $x_{12d} = -0.35\sin(0.6t)rad$ are employed to verify the applicability of the PFTO-ABSTC. The trajectory tracking results of different control methods are shown in Fig. 4, and the tracking errors generated during the tracking process are shown in Fig. 5. In addition, the performance indices of tracking errors generated by different control methods are shown in Table I. Due to controller C4 ignores the dynamics of the DHM completely, it generates the largest tracking error during the tracking process. The controller C3 is designed based on the dynamic model of the DHM, and the influence of the parameter uncertainty of the system is further considered, the maximum tracking accuracy generated is improved by about 30% compared with C4. However, the above improvement is still difficult

TABLE I
PERFORMANCE INDICES OF THE FOUR CONTROLLERS IN CASE 1

Joint	Methods	AME	MSE	SD
Rotary	C1	1.41×10^{-2}	1.57×10^{-5}	4.01×10^{-3}
	C2	2.44×10^{-2}	4.70×10^{-5}	6.90×10^{-3}
	C3	2.97×10^{-2}	6.81×10^{-5}	8.35×10^{-3}
	C4	4.23×10^{-2}	4.99×10^{-4}	2.03×10^{-2}
Pitch	C1	1.27×10^{-2}	9.37×10^{-6}	3.10×10^{-3}
	C2	2.26×10^{-2}	3.76×10^{-5}	6.15×10^{-3}
	C3	2.72×10^{-2}	6.13×10^{-5}	7.81×10^{-3}
	C4	4.14×10^{-2}	6.19×10^{-4}	2.48×10^{-2}

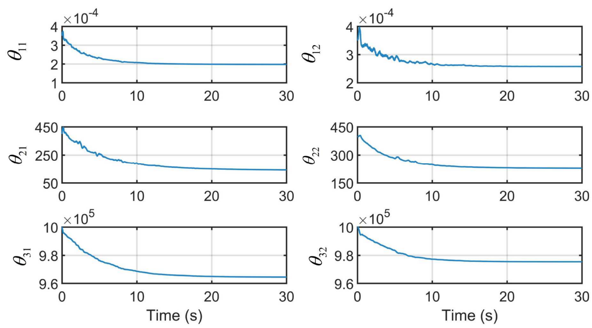

Fig. 6. Parameters adaptive results in Case 1.

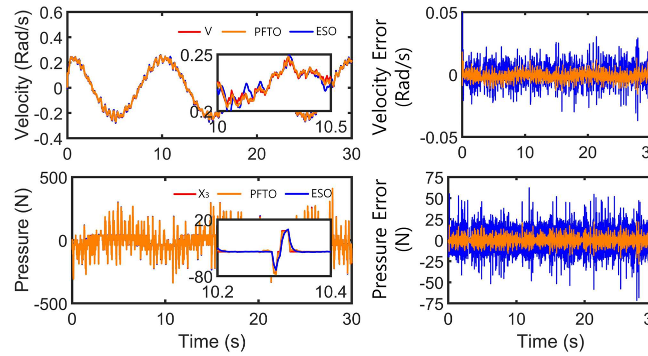

Fig. 7. State estimation results of Rotary Joint in Case 1.

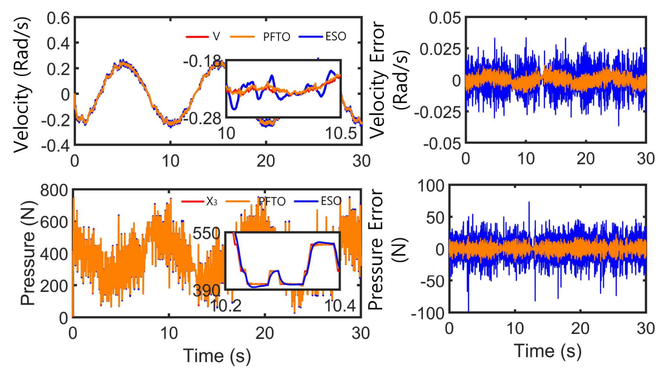

Fig. 8. State estimation results of Pitch Joint in Case 1.

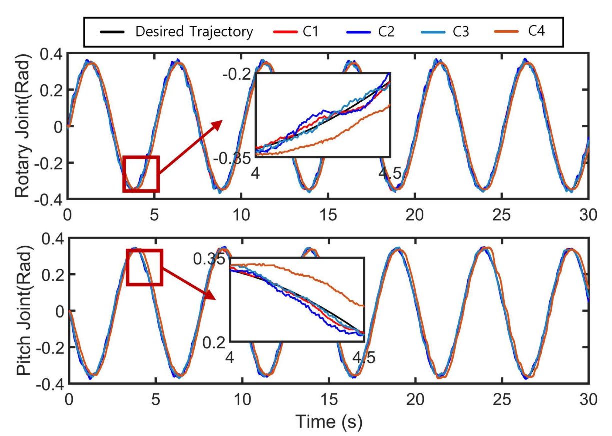

Fig. 9. Trajectory tracking results of the four controllers in Case 1.

to meet expectations, which is due to the inevitable existence of lots of internal and external disturbances, such as pressure shock disturbance and internal friction. Thus, in order to compensate for the above disturbance, controller C2 is constructed based on C3 controller by integrating ESOs. It can be seen from the data in Table I that all data performance indices of tracking error have been improved. However, because these ESOs can only achieve asymptotic convergence and easily amplify system noise, only limited performance improvement can be achieved. It is worth noting that controller C1 achieves the minimum trajectory tracking error by integrating PFTO strategy, which is at least 42.21%, 52.53%, and 66.67% smaller than other control methods, respectively. In addition, the MSE and SD indices of the C1 are significantly improved compared to other control methods. The results of the parameter adaptive law can be seen in Fig. 6. The state estimation results obtained by PFTOs and ESOs are shown in Figs. 7 and 8. It can be seen that both strategies can converge to the bounded neighborhood of the system state. However, according to the subfigures and error analysis, compared with ESO, PFTO strategy can make the estimator converge better to the state through the design of a disturbance adaptive term and a fractional-order term in the presence of multiple source disturbances, so that controller C1 can obtain better control performance.

*Case*2: The high-speed sine trajectory $x_{11d} = 0.35 \sin(1.25t)rad$ and $x_{12d} = -0.35 \sin(1.25t)rad$ is used to further test the performance of the different controllers. The trajectory tracking results and errors obtained by different controllers are shown in Figs. 9 and 10, respectively. The performance indices of trajectory tracking errors are shown in Table II. It can be seen from the above results that the trajectory tracking error obtained by controller C1 is still smaller than that of other controllers, and the maximum trajectory tracking error is increased by at least 41.30%, 50.76%, and 71.66% respectively. As can be seen from Figs. 11 and 12, the PFTO strategy proposed in this article still achieves better state estimation effect than the ESO strategy, and converges to the bounded neighborhood of the system state with a smaller state estimation error. In addition, the controller C1 obtains smaller MSE and SD compared with other controllers according to the Table II. By comparing controllers C1 and C2, the difference is only in the ESOs and PFTOs strategies, while

This article has been accepted for inclusion in a future issue of this journal. Content is final as presented, with the exception of pagination.

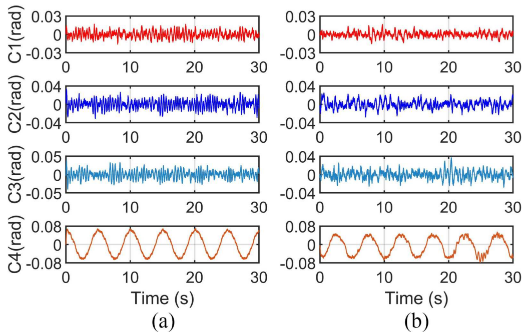

Fig. 10. Trajectory tracking errors of the four controllers in Case 2. (a) Rotary Joint. (b) Pitch Joint.

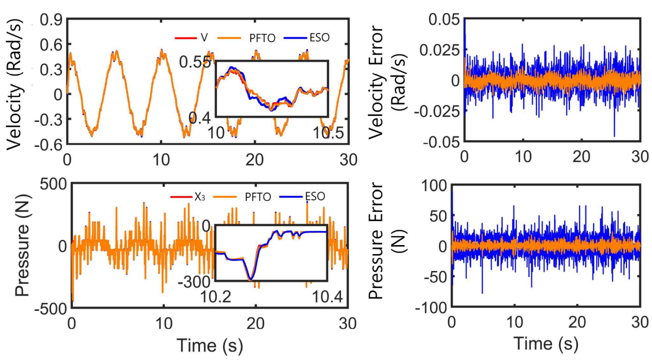

Fig. 11. State estimation results of Rotary Joint in Case 2.

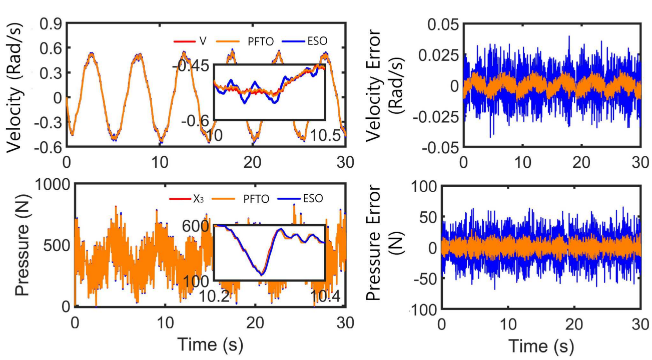

Fig. 12. State estimation results of Pitch Joint in Case 2.

TABLE II
PERFORMANCE INDICES OF THE FOUR CONTROLLERS IN CASE 2

Joint	Methods	AME	MSE	SD
Rotary	C1	1.89×10^{-2}	2.65×10^{-5}	5.10×10^{-3}
	C2	3.29×10^{-2}	7.85×10^{-5}	8.92×10^{-3}
	C3	3.96×10^{-2}	1.14×10^{-4}	1.12×10^{-2}
	C4	6.12×10^{-2}	1.52×10^{-3}	3.90×10^{-2}
Pitch	C1	1.62×10^{-2}	1.76×10^{-5}	4.20×10^{-3}
	C2	2.76×10^{-2}	6.51×10^{-5}	8.10×10^{-3}
	C3	3.67×10^{-2}	9.89×10^{-5}	1.05×10^{-2}
	C4	7.78×10^{-2}	1.41×10^{-3}	3.64×10^{-2}

the MSE and SD of C1 controller have been greatly improved, which also proves the effectiveness and excellence of PFTO strategies.

V. CONCLUSION

This article addresses the trajectory tracking control of a DHM with unknown disturbances and parameter uncertainties. An PFTO-ABSTC method was proposed to ensure the asymptotic stability of the tracking error. First, a projection-type adaptive law was employed to estimate the system's uncertain parameters. Second, the PFTO was developed to estimate and compensate for disturbances. By integrating the PFTO and the adaptive law, the PFTO-ABSTC controller was constructed. The stability of the closed-loop system was proven via Lyapunov stability theory. Finally, the control performance of the proposed controller was demonstrated through experimental results performed on a 2-DOF DHM. In future work, we plan to conduct experiments with more degrees of freedom and to further consider the actual physical constraints of the system.

A. Proof of Theorem 1

Define $\vartheta = [\tilde{x}_{i+1}, \tilde{\eta}_i]^T, i = 1, 2$. And choose Lyapunov function as follows:

$$V_1 = \vartheta^T \mathrm{diag}\left[\frac{\omega_1}{2}, \frac{1}{2}\right]\vartheta = \frac{\omega_1}{2}\tilde{x}_{i+1}^2 + \frac{1}{2}\tilde{\eta}_i^2 \tag{A.1}$$

Derivative the (A.1) can obtain

$$\begin{aligned}\dot{V}_1 &= \omega_1 \tilde{x}_{i+1}\dot{\tilde{x}}_{i+1} + \tilde{\eta}_i \dot{\tilde{\eta}}_i \\ &= \omega_1 \tilde{x}_{i+1}(\tilde{\eta}_i - k_{f1}\tilde{x}_{i+1} - k_{f2}|\tilde{x}_{i+1}|^{(r-1)/r} sign(\tilde{x}_{i+1})) \\ &\quad + \tilde{\eta}_i(\dot{\eta}_i - \omega_1 \tilde{x}_{i+1} + \omega_2 \eta_i - \omega_2 \tilde{\eta}_i) \\ &\le -k_{f1}\omega_1 \tilde{x}_{i+1}^2 - k_{f2}\omega_1 \tilde{x}_{i+1}^{(2r-1)/r} + \omega_1 \tilde{x}_{i+1}\tilde{\eta}_i \\ &\quad + (\omega_2 D_1 + D_2)\tilde{\eta}_i - \omega_1 \tilde{x}_{i+1}\tilde{\eta}_i - \omega_2 \tilde{\eta}_i^2 \\ &= -k_{f1}\omega_1 \tilde{x}_{i+1}^2 - k_{f2}\omega_1 \tilde{x}_{i+1}^{(2r-1)/r} - \omega_2 \tilde{\eta}_i^2 + (\omega_2 D_1 + D_2)\tilde{\eta}_i \\ &= -\vartheta^T \mathrm{diag}[k_{f1}\omega_1, \omega_2]\vartheta - k_{f2}\omega_1 \tilde{x}_{i+1}^{(2r-1)/r} + (\omega_2 D_1 + D_2)\tilde{\eta}_i\end{aligned} \tag{A.2}$$

By Lemma 3, we have

$$\begin{aligned}\dot{V}_1 \le &-\left(\frac{4rk_{f1}\omega_1}{(2r-1)\lambda_1} + k_{f2}\omega_1\right)|\tilde{x}_{i+1}|^{(2r-1)/r} \\ &- \frac{4r\omega_2}{(2r-1)\lambda_2}|\tilde{\eta}_i|^{(2r-1)/r} \\ &+ (\omega_2 D_1 + D_2)\tilde{\eta}_i + \frac{k_{f1}\omega_1}{4r\lambda_1^{2r-1}} + \frac{\omega_2}{4r\lambda_2^{2r-1}} \\ \le &-\varsigma V_1^{(2r-1)/2r} + \nabla\end{aligned} \tag{A.3}$$

where $\lambda_1 = (m-1)/2m$, $\lambda_2 = 1/2m$, $\ell_1 = 1$, $\varsigma = \min\{((4rk_{f1}\omega_1/(2r-1)\lambda_1) + k_{f2}\omega_1), (4r\omega_2/(2r-1)\lambda_2)\}$ and $\nabla = (\omega_2 D_1 + D_2)\tilde{\eta}_i + (k_{f1}\omega_1/4r\lambda_1^{2r-1}) + (\omega_2/4r\lambda_2^{2r-1})$.

According to Lemma 2, the state estimation error $\tilde{x}_{i+1}$ of the observer can converge to zero in practical finite-time t_{PFTO}. Since then, the finite-time convergence of the observer has been proven.

B. Proof of Theorem 2

Substituting α_2 and u into (22) and (27), we can obtain as follows:

$$\dot{s}_1 = -k_{11}s_1 - k_{12}|s_1|^{1/2} sign(s_1) + \alpha_{aux} + d_1$$

$$\begin{aligned}&\dot{\alpha}_{aux} + \Im_1 \alpha_{aux} = -k_{13} sign(s_1) && \text{(A.4)}\\ &\dot{s}_2 = -k_{21}s_2 - k_{22}|s_2|^{1/2} sign(s_2) + u_{aux} + d_2 \\ &\dot{u}_{aux} + \Im_2 u_{aux} = -k_{23} sign(s_2) && \text{(A.5)}\end{aligned}$$

where $d_1 = \phi_1 \xi_2 + \tilde{f}_1 + \hat{\theta}_2 z_3$, $d_2 = \hat{\theta}_2 \phi_4 \xi_2 + \tilde{f}_2$. To maintain generality and facilitate subsequent analysis, the above formulas are rewritten in the following form:

$$\begin{aligned}&\dot{s}_i = -k_{i1}s_i - k_{i2}|s_i|^{1/2} sign(s_i) + m_i \\ &\dot{m}_i + \Im_i m_i = -k_{i3} sign(s_i) + \dot{d}_i && \text{(A.6)}\end{aligned}$$

where $i = 1, 2$, $m_1 = \alpha_{aux} + d_1$, $m_2 = u_{aux} + d_2$. Define vector $\hbar_i = [|s_i|^{1/2} sign(s_i) \quad s_i \quad m_i\ ]^T$, and consider Lyapunov function as follows:

$$\begin{aligned}V_{2i} = &\varpi_{1i}|s_i| + \varpi_{2i}s_i^2 + \varpi_{3i}m_i \\ &+ \frac{1}{2}(k_{i1}s_i + k_{i2}|s_i|^{1/2} sign(s_i) - m_i)^2 \qquad \text{(A.7)}\end{aligned}$$

where $\varpi_{ji} > 0$, $j = 1, 2, 3$. Obviously, the Lyapunov function above is continuous and differentiable in $V_{2i} \in \{V_{2i}(s_i, m_i) | s_i \neq 0\}$. Therefore, differentiating (A.7) yields the following:

$$\begin{aligned}\dot{V}_{2i} = &\varpi_{1i}\frac{s_i}{|s_i|}\dot{s}_i + 2\varpi_{2i}s_i\dot{s}_i + 2\varpi_{3i}m_i\dot{m}_i \\ &+ (k_{i1}s_i + k_{i2}|s_i|^{1/2} sign(s_i) - m_i)\left(k_{i1}\dot{s}_i + k_{i2}\frac{\dot{s}_i}{|s_i|^{1/2}} - \dot{m}_i\right)^2 \qquad \text{(A.8)}\end{aligned}$$

Substituting (A.6) into (A.8) gives as follows:

$$\begin{aligned}\dot{V}_{2i} \leq &(k_{i1}k_{i2}^2 + k_{i1}k_{i3} - k_{i1}\varpi_{1i} + k_{i1}D)|s_i| \\ &- (k_{i2}\varpi_{1i} + k_{i2}^3 + k_{i2}k_{i3} + k_{i2}D)|s_i|^{1/2} \\ &+ (\varpi_{1i} + 2k_{i3}\varpi_{3i} - k_{i3} + 2\varpi_{3i}D + D)|m_i| \\ &- (2k_{i1}\varpi_{2i} + k_{i1}^3)s^2 - (2k_{i2}\varpi_{2i} - k_{i1}k_{i2})|s_i|^{3/2} \\ &+ (2\varpi_{2i} + 2k_{i1}^2 + k_{i1}\Im_i)|s_i||m_i| \\ &- (2\Im_i\varpi_{3i} - k_{i1} - \Im_i)m_i^2 \\ &+ (2k_{i1}k_{i2} + k_{i2}\Im_i)|s_i|^{1/2}|m_i| + k_{i2}\frac{m_i^2}{|s_i|^{1/2}} \qquad \text{(A.9)}\end{aligned}$$

Thus, (A.9) can be rewritten as

$$\dot{V}_{2i} \leq -\hbar_i^T \Upsilon_{1i}\hbar_i - \frac{1}{|s_i|^{1/2}}\hbar_i^T \Upsilon_{2i}\hbar_i \qquad \text{(A.10)}$$

According to the assumption in (28) and (29), both Υ_{1i} and Υ_{2i} are positive definite matrices. Therefore, according to the properties of positive definite matrices, we can obtain as follows:

$$\begin{aligned}&\lambda_{\min}(\Upsilon_{1i})\|\hbar_i\|_2^2 \leq \hbar_i^T\Upsilon_{1i}\hbar_i \leq \lambda_{\max}(\Upsilon_{1i})\|\hbar_i\|_2^2 \\ &\lambda_{\min}(\Upsilon_{2i})\|\hbar_i\|_2^2 \leq \hbar_i^T\Upsilon_{2i}\hbar_i \leq \lambda_{\max}(\Upsilon_{2i})\|\hbar_i\|_2^2 \qquad \text{(A.11)}\end{aligned}$$

Then, (A.10) can be further rewritten as

$$\dot{V}_{2i} \leq -\lambda_{\min}(\Upsilon_{1i})\|\hbar_i\|_2^2 - \frac{1}{|s_i|^{1/2}}\lambda_{\min}(\Upsilon_{2i})\|\hbar_i\|_2^2 \qquad \text{(A.12)}$$

According to (A.7), we can obtain as follows

$$\begin{aligned}&\lambda_{\min}(\Phi_i)\|\hbar_i\|_2^2 \leq V_{2i} \leq \lambda_{\max}(\Phi_i)\|\hbar_i\|_2^2 \\ &|s_i|^{1/2} \leq \|\hbar_i\| \leq \frac{V_{2i}^{1/2}}{\lambda_{\min}^{1/2}(\Phi_i)} \qquad \text{(A.13)}\end{aligned}$$

where the positive-definite matrix Φ_i is given by

$$\Phi_i = \frac{1}{2}\begin{bmatrix} 2\varpi_{1i} + k_{i2}^2 & k_{i1}k_{i2} & -k_{i2} \\ k_{i1}k_{i2} & 2\varpi_{2i} + k_{i1}^2 & -k_{i1} \\ -k_{i2} & -k_{i1} & 2\varpi_{3i} + 1 \end{bmatrix} \qquad \text{(A.14)}$$

Thus,

$$\dot{V}_{2i} \leq -\frac{\lambda_{\min}(\Upsilon_{1i})}{\lambda_{\max}(\Phi_i)}V_{2i} - \frac{\lambda_{\min}^{1/2}(\Phi_i)\lambda_{\min}(\Upsilon_{2i})}{\lambda_{\max}(\Phi_i)}V_{2i}^{1/2} \qquad \text{(A.15)}$$

According to Lemma 15 in [28], the sliding mode manifold converge to zero in finite time. Thus, Theorem 2 is proven.

C. Proof of Theorem 3

The Lyapunov function is as follows:

$$V_3 = \frac{1}{2}z_1^T z_1 + \frac{1}{2}z_2^T z_2 + \frac{1}{2}z_3^T z_3 + \frac{1}{2}\tilde{\Theta}^T\Gamma^{-1}\tilde{\Theta} + V_1 + V_{21} + V_{22} \qquad \text{(A.16)}$$

Combined with (10), (19), (23), (28), (29), (A.1), (A.7), (A.11), and (A.15), the derivative of V_3 can be obtained as

$$\begin{aligned}\dot{V}_3 \leq &- k_1\|z_1\|^2 - a_1\|z_2\|^2 - a_2\|z_3\|^2 \\ &+ |z_1||z_2| + k_{11}|z_2||s_1| + k_{12}|z_2||s_1|^{1/2} \\ &- \lambda_{\min}(\psi)\left\|\tilde{\Theta}\right\|^2 + \lambda_{\max}(\psi)\left\|\tilde{\Theta}^T\Theta\right\| \\ &+ |z_2||m_1| + k_{21}|z_3||s_2| + k_{22}|z_3||s_2|^{1/2} \\ &+ |z_3||m_2| + V_1 + V_{21} + V_{22} + \left|\hat{\theta}_2\phi_4 x_2\right| + |\phi_1 x_2| \qquad \text{(A.17)}\end{aligned}$$

Define vectors $z = [|z_1| \quad |z_2| \quad |z_3|]^T$, $\hbar_1 = [|s_1|^{1/2} \quad |s_1| \quad |m_1|]^T$, $\hbar_2 = [|s_2|^{1/2} \quad |s_2| \quad |m_2|]^T$, and $\chi = [z \quad \vartheta \quad \hbar_1 \quad 0 \quad \hbar_2 \quad \tilde{\Theta}]^T$. With the definition of Λ, the above equation can be further rewritten as

$$\begin{aligned}\dot{V}_3 &\leq -\chi^T\Lambda\chi + \Delta \\ &\leq -\lambda_{\min}(\Lambda)V_3 + \Delta \qquad \text{(A.18)}\end{aligned}$$

where $\Delta = |(\lambda_{\min}^{1/2}(\Phi_1)\lambda_{\min}(\Upsilon_{21})/\lambda_{\max}(\Phi_1))V_{21}^{1/2} + (\lambda_{\min}^{1/2}(\Phi_2)\lambda_{\min}(\Upsilon_{22})/\lambda_{\max}(\Phi_2))V_{22}^{1/2} + \left|\hat{\theta}_2\phi_4 x_2\right| + |\phi_1 x_2| + \lambda_{\max}(\psi)\left\|\tilde{\Theta}^T\Theta\right\| + k_{f2}\omega_1\tilde{x}_{i+1}^{(2r-1)/r} + (\omega_2 D_1 + D_2)\tilde{\eta}_i|$. Obviously, Δ is bounded and V_3 is also bounded; thus, the error z is also bounded. Then, according to the assumption, the state x of the closed loop system is also bounded, so all the signals of the whole system are bounded.

References

[1] S. Zhou, C. Shen, Y. Xia, Z. Chen, and S. Zhu, "Adaptive robust control design for underwater multi-dof hydraulic manipulator," *Ocean Eng.*, vol. 248, p. 110822, Mar. 2022.

[2] C. Gang et al., "Dynamic tail modeling and motion analysis of a beaver-like robot," *Nonlinear Dyn.*, vol. 112, pp. 6859–6875, Mar. 2024.

[3] Z. Chen, B. Helian, Y. Zhou, and M. Geimer, "An integrated trajectory planning and motion control strategy of a variable rotational speed pump-controlled electro-hydraulic actuator," *IEEE/ASME Trans. Mechatron.*, vol. 28, no. 1, pp. 588–597, Feb. 2023.

[4] H. Feng, C. Yin, and D. Cao, "Trajectory tracking of an electro-hydraulic servo system with an new friction model-based compensation," *IEEE/ASME Trans. Mechatron.*, vol. 28, no. 1, pp. 473–482, Feb. 2023.

[5] C. Li, L. Lyu, B. Helian, Z. Chen, and B. Yao, "Precision motion control of an independent metering hydraulic system with nonlinear flow modeling and compensation," *IEEE Trans. Ind. Electron.*, vol. 69, no. 7, pp. 7088–7098, Jul. 2022.

[6] H. Du, L. Wang, J. Chen, H. Huang, and X. Feng, "Integral sliding-mode tracking control for heavy vehicle electrohydraulic power steering system," *IEEE/ASME Trans. Mechatron.*, vol. 26, no. 3, pp. 1455–1466, Jun. 2021.

[7] Y. Xia et al., "Advanced motion control of hydraulic manipulator with precise compensation of dynamic friction," *IEEE Trans. Ind. Inform.*, vol. 20, no. 7, pp. 9375–9384, Jul. 2024.

[8] C. Yang, Y. Jiang, W. He, J. Na, Z. Li, and B. Xu, "Adaptive parameter estimation and control design for robot manipulators with finite-time convergence," *IEEE Trans. Ind. Electron.*, vol. 65, no. 10, pp. 8112–8123, Oct. 2018.

[9] S. Wang and J. Na, "Parameter estimation and adaptive control for servo mechanisms with friction compensation," *IEEE Trans. Ind. Inform.*, vol. 16, no. 11, pp. 6816–6825, Nov. 2020.

[10] J. Chen, L. Lyu, Z. Fei, W. Xia, and X.-M. Sun, "Event-triggered adaptive robust control for a class of uncertain nonlinear systems with application to mechatronic system," *IEEE Trans. Ind. Inform.*, vol. 19, no. 12, pp. 11800–11808, Dec. 2023.

[11] W. Deng and J. Yao, "Adaptive integral robust control and application to electromechanical servo systems," *ISA Trans.*, vol. 67, pp. 256–265, Mar. 2017.

[12] Y. Ma, T. Qin, and Y. Li, "Nonlinear extended state observer based super-twisting terminal sliding mode synchronous control for parallel drive systems," *IEEE/ASME Trans. Mechatron.*, vol. 28, no. 6, pp. 3087–3098, Dec. 2023.

[13] D. Fan and G. Guan, "Random vibration model reference sliding mode control of electro-hydraulic shaking table based on linear state observer," in *Proc. 7th Int. Conf. Automat., Control Robot. Eng. (CACRE)*, 2022, pp. 172–177.

[14] Z. Wan, L. Yue, and Y. Fu, "Neural network based adaptive backstepping control for electro-hydraulic servo system position tracking," *Int. J. Aerosp. Eng.*, vol. 27, pp. 1–16, Sep. 2022.

[15] Y. Ge, J. Zhou, W. Deng, J. Yao, and L. Xie, "Neural network robust control of a 3-DOF hydraulic manipulator with asymptotic tracking," *Asian J. Control*, vol. 25, no. 3, pp. 2060–2073, Jun. 2023.

[16] K. Guo, M. Li, W. Shi, and Y. Pan, "Adaptive tracking control of hydraulic systems with improved parameter convergence," *IEEE Trans. Ind. Electron.*, vol. 69, no. 7, pp. 7140–7150, Jul. 2022.

[17] J. Yao, W. Deng, and Z. Jiao, "Adaptive control of hydraulic actuators with lugre model-based friction compensation," *IEEE Trans. Ind. Electron.*, vol. 62, no. 10, pp. 6469–6477, Oct. 2015.

[18] J. Yao and W. Deng, "Active disturbance rejection adaptive control of hydraulic servo systems," *IEEE Trans. Ind. Electron.*, vol. 64, no. 10, pp. 8023–8032, Oct. 2017.

[19] Z. Yan, S. Deng, Z. Yang, Y. Wang, Y. Lu, and X. Shi, "An ADRC strategy with sequential output stacking extended state observers to evaluate hydraulic torque for a continuous-wave pulse generator," *IEEE Trans. Ind. Inform.*, vol. 20, no. 3, pp. 4259–4270, Mar. 2024.

[20] Z. Zhang, Y. Guo, D. Gong, and J. Liu, "Global integral sliding-mode control with improved nonlinear extended state observer for rotary tracking of a hydraulic roofbolter," *IEEE/ASME Trans. Mechatron.*, vol. 28, no. 1, pp. 483–494, Feb. 2023.

[21] D. Won, W. Kim, and M. Tomizuka, "High-gain-observer-based integral sliding mode control for position tracking of electrohydraulic servo systems," *IEEE/ASME Trans. Mechatron.*, vol. 22, no. 6, pp. 2695–2704, Dec. 2017.

[22] Q. Hou, S. Ding, and X. Yu, "Composite super-twisting sliding mode control design for PMSM speed regulation problem based on a novel disturbance observer," *IEEE Trans. Energy Convers.*, vol. 36, no. 4, pp. 2591–2599, Dec. 2021.

[23] X. Yang, J. Yao, and W. Deng, "Output feedback adaptive super-twisting sliding mode control of hydraulic systems with disturbance compensation," *ISA Trans.*, vol. 109, pp. 175–185, Feb. 2021.

[24] S. Park and S. Han, "Robust super-twisting sliding mode backstepping control blended with tracking differentiator and nonlinear disturbance observer for an unknown UAV system," *Appl. Sci.*, vol. 12, no. 5, p. 2490, Feb. 2022.

[25] H. Peng, B. Huang, M. Jin, C. Zhu, and J. Zhuang, "Distributed finite-time bearing-based formation control for underactuated surface vessels with levant differentiator," *ISA Trans.*, vol. 147, pp. 239–251, Apr. 2024.

[26] W. Deng and J. Yao, "Extended-state-observer-based adaptive control of electrohydraulic servomechanisms without velocity measurement," *IEEE/ASME Trans. Mechatron.*, vol. 25, no. 3, pp. 1151–1161, Jun. 2020.

[27] W. Lin et al., "Adaptive extended state observer-based velocity-free servo tracking control with friction compensation," *IEEE Trans. Syst., Man, Cybern.: Syst.*, vol. 54, no. 1, pp. 2–11, Jan. 2024.

[28] K. Wang, X. Liu, and Y. Jing, "Adaptive finite-time command filtered controller design for nonlinear systems with output constraints and input nonlinearities," *IEEE Trans. Neural Netw. Learn. Syst.*, vol. 33, no. 11, pp. 6893–6904, Nov. 2022.

[29] Y. Fei, P. Shi, C. P. Lim, and X. Yuan, "Finite-time observer-based formation tracking with application to omnidirectional robots," *IEEE Trans. Ind. Electron.*, vol. 70, no. 10, pp. 10598–10606, Oct. 2023.

Gang Chen (Member, IEEE) received the Ph.D. degree in mechatronic engineering from the State Key Laboratory of Fluid Power and Mechatronic Systems, Zhejiang University, Hangzhou, China, in 2014.

Currently, he is a Professor with the School of Mechanical Engineering, Zhejiang Sci-Tech University. His research interests include bionic robots, motion analysis and planning, and intelligent control.

Wei Wu (Student Member, IEEE) received the B.E. degree in 2022 in mechanical and electronic engineering from the School of Mechanical Engineering, Zhejiang Sci-Tech University, Hangzhou, China, where he is currently working toward the master's degree in mechanical engineering.

His research interests include sliding mode control theory and applications, electro-hydraulic servo system, robot manipulator control, and nonlinear system control.

Chenguang Yang (Fellow, IEEE) received the B.Eng. degree in measurement and control from Northwestern Polytechnical University, Xi'an, China, in 2005, and the Ph.D. degree in control engineering from the National University of Singapore, Singapore, in 2010.

He performed postdoctoral studies in human robotics with Imperial College London, London, U.K., from 2009 to 2010. He holds the Chair in robotics with the Department of Computer Science, University of Liverpool, Liverpool, U.K. He is leading the Robotics and Autonomous Systems Group. He was leading Robot Teleoperation Group, Bristol Robotics Laboratory, Bristol, UK. His research interest include robot control and learning, human robot interaction, and intelligent system design.

Dr. Yang is a member of European Academy of Sciences and Arts (EASA), Salzburg, Austria. He was awarded UK EPSRC UKRI Innovation Fellowship and individual EU Marie Curie International Incoming Fellowship. He was the President of Chinese Automation and Computing Society, London, U.K. He is the Corresponding Co-Chair of IEEE Technical Committee on Collaborative Automation for Flexible Manufacturing.

As the Lead Author, he won the IEEE TRANSACTIONS ON ROBOTICS Best Paper Award (2012) and IEEE TRANSACTIONS ON NEURAL NETWORKS AND LEARNING SYSTEMS Outstanding Paper Award (2022).

Huosheng Hu (Life Senior Member, IEEE) received the M.Sc. degree in industrial automation from the Central South University, Changsha, China, in 1982, and the Ph.D. degree in robotics from the University of Oxford, Oxford, U.K., in 1993.

Currently, he is a Professor with the School of Computer Science and Electronic Engineering, University of Essex, Colchester, U.K., where he is leading the Robotics Research Group. He has authored or co-authored more than 420 articles. His research interests include robotics, humanârobot interaction, embedded systems, mechatronics, and pervasive computing.

Prof. Hu is a Founding Member of the IEEE Robotics and Automation Society Technical Committee on Networked Robots, a fellow of the Institution of Engineering and Technology, and a Senior Member of the Association for Computing Machinery. He currently serves as an Editor-in-Chief of the *International Journal of Automation and Computing* and the online *Robotics* journal and an Executive Editor of the *International Journal of Mechatronics and Automation*.

Jingjing Zhang received the master's degree in computer application technology from Guangxi Minzu University, Nanning, China, in 2010. He is the VP of ZheJiang CathayBot Technology Company Ltd., Jinhua, China. He has been working on special robot research for over 13 years.

Jianwei Shi master's degree in electrical automation from the Southwest Jiaotong University, Chengdu, China, in 1998. He is a RD Engineer with Zhejiang Cathaybot Technology Company Ltd., Jinhua, China, who is responsible for the hardware research and development of hydraulic robotic arm control system and has been working on hardware and software of automatic microcontrollers for over 20 years.

Chuanyu Wu received the Ph.D. degree in mechanical engineering from Zhejiang University, Hangzhou, China, in 2002.

He became a Lecturer in 2002, an Associate Professor in 2004, and a Professor in 2008 with Zhejiang Sci-Tech University, Zhejiang, China. In 2016, he was a Visiting Scholar with the University of Houston, Texas, USA. Currently, he is a Professor with Zhejiang Ocean University, Zhoushan, China. His research interests include smart structures, robotics, machine design and application, and intelligent equipment.

Yu Ma received the Ph.D. degree in computer science and technology from the Northwestern Polytechnical University, Shaanxi, China, in 2013.

Currently, he is a Professor with the Department of Electrical and Electronic Engineering, Ningxia University, Yinchuan, China. His research interests include computer vision and pattern recognition.